THE UNIVERSITY of EDINBURGH

Edinburgh Research Explorer

Pretensioned centrifugal spun high-strength concrete piles reinforced with steel strands: flexural performances

Link:
Link to publication record in Edinburgh Research Explorer

Document Version:
Peer reviewed version

Published In:
Magazine of Concrete Research

OPEN ACCESS

1 **Pretensioned centrifugal spun high-strength concrete piles reinforced with steel**

2 **strands: flexural performances**

3 **Xuwei Zhang**

4 Postgraduate Student, Department of Civil Engineering, Zhejiang University, Hangzhou, China

5 **Shunfeng Gong**

6 Professor, Department of Civil Engineering, Zhejiang University, Hangzhou, China (corresponding

7 author: sfgong@zju.edu.cn)

8 **Quanbiao Xu**

9 Senior Engineer, Center for Balance Architecture, Zhejiang University; Architectural Design &

10 Research Institute of Zhejiang University Co. Ltd, Hangzhou, China

11 **Gang Gan**

12 Senior Engineer, Center for Balance Architecture, Zhejiang University; Architectural Design &

13 Research Institute of Zhejiang University Co. Ltd, Hangzhou, China

14 **Xiaodong Yu**

15 Engineer, Ningbo Yizhong Concrete Pile Co. Ltd, Ningbo, China

16 **Yong Lu**

17 Professor, Institute for Infrastructure and Environment, School of Engineering, University of

18 Edinburgh, Edinburgh, United Kingdom

1

1   **Abstract:** The application of pretensioned spun high-strength concrete (PHC) piles in high intensity

2   seismic areas has so far been limited by insufficient horizontal load resistance and poor deformation

3   capacity. A new type of pretensioned spun concrete pile with high strength and high elongation steel

4   strands instead of steel bars has been developed. This paper presents the flexural performance

5   evaluation of the new centrifugal spun concrete pile with steel strands (hereafter referred to as PSC

6   pile). An experimental study is presented first, including the bending tests on six full-scale pile test

7   specimens with three different pile diameters. The flexural performances of PHC and PSC piles are

8   comparatively assessed in terms of crack resistance, ultimate bearing capacity, deformation capacity

9   and failure mode. The results show that the new PSC piles have similar crack resistance, but higher

10   ultimate bearing capacity and better deformation capacity under a flexural condition. Comparing to

11   PHC piles which exhibit a brittle bending failure due to the rupture of prestressing steel bars, PSC

12   piles demonstrate a ductile bending failure with a more gradual crushing of concrete in the

13   compression zone. Following the experimental study, a theoretical model is developed to evaluate the

14   flexural strength of the piles, and a simplified calculation equation for ultimate bending moment is

15   proposed. Finally, a finite element model is also established to simulate the flexural performance of

16   the piles and the modelling results are found to be in good agreement with the experimental results.

17   **Keywords:** pretensioned spun concrete piles; prestressing strand; flexural performance; failure mode;

18   theoretical analysis; finite element model

19   **Notation**

20   A cross-section area of pile, mm^2

21   A_p total cross-section area of prestressing tendons, mm^2

22   D_1 external diameter of pile section, mm

2

1	D_2	internal diameter of pile section, mm
2	D_p	diameter of the circle at the centre of prestressing tendons, mm
3	E_c	elastic modulus of concrete, MPa
4	E_s	elastic modulus of reinforcing bar, GPa
5	f_c	axial compressive strength of concrete, MPa
6	f_{cu}	compressive strength of 150 mm ×150 mm×150 mm concrete cube, MPa
7	$f_{cu,10}$	compressive strength of 100 mm ×100 mm×100 mm concrete cube, MPa
8	f_{pt}	tensile strength of prestressing tendon, MPa
9	f_t	tensile strength of concrete, Mpa
10	f_y	yield strength of reinforcing bar, MPa
11	f_u	ultimate tensile strength of reinforcing bar, MPa
12	$f_{u,e}$	experimental value of maximum midspan deflexion, mm
13	$f_{u,n}$	numerical value of maximum midspan deflexion, mm
14	h	depth of neutral axis, mm
15	L	length of pile, mm
16	M_e	experimental bending moment of midspan section, kN·m
17	$M_{cr,e}$	experimental value of cracking moment, kN·m
18	$M_{cr,n}$	numerical value of cracking moment, kN·m
19	$M_{u,e}$	experimental value of ultimate bending moment, kN·m
20	$M_{u,n}$	numerical value of ultimate bending moment, kN·m
21	r_1	external radius of pile section, mm
22	r_2	internal radius of pile section, mm

3

1 r_p radius of the circle at the centre of prestressing tendons, mm

2 t wall thickness of pile, mm

3 W self-weight of pile, kN

4 δ maximum force elongation of reinforcing bar

5 ε_{cm} peak compressive strain of concrete

6 ε_{tm} peak tensile strain of concrete

7 ε_y yield strain of reinforcing bar

8 ρ_s ratio of longitudinal reinforcement

9 σ_{ce} effective compressive pre-stress of concrete, MPa

10 σ_{con} tensile control stress of prestressing tendon, MPa

11 σ_{cm} peak compressive strength of concrete, MPa

12 σ_{p0} initial stress of prestressing tendon, MPa

13 σ_{tm} peak tensile strength of concrete, MPa

14 1. Introduction and research significance

15 Pretensioned spun high-strength concrete (PHC) piles are fabricated by pretensioned prestressing

16 technology and usually using a centrifugal forming method, and have been widely used in foundation

17 engineering with the advantages of high bearing capacity, reliable quality assurance, simple

18 manufacture process and outstanding economic benefit. PHC piles are often used to support large

19 superstructures when the ground soil conditions are not strong enough, and they also need to bear

20 lateral loads caused by wind, wave and earthquake. The investigation of pile damage in 1995

21 Hyougoken-Nanbu earthquake in Japan showed that PHC piles had poor seismic performance and

22 suffered brittle failure at the pile heads under the seismic loading (Nagae and Hayashi, 2003).

4

Furthermore, the collapse incident of a 13-story building in Shanghai in 2009 raised more concerns about the horizontal bearing capacity of PHC piles (Wang *et al*., 2017). Improving the horizontal bearing capacity and deformation capacity of PHC piles becomes an urgent call.

PHC piles were first developed in Japan and subsequently introduced to China, which have gradually become the main type of prestressed concrete piles in the two countries. In order to improve the strength and ductility of PHC piles and make them suitable for application in seismic areas, scholars from both countries have carried out a lot of research in the last two decades. Kishida *et al*. (2000) investigated the ultimate shear behaviour of PHC piles and the influence of increasing spiral reinforcement ratio and adding concrete infilling, and the results showed that using both methods could improve ultimate strength and deformation behaviour but using the concrete infilling alone could not prevent the brittle failure. Then, Nagae and Hayashi (2003) studied the seismic performance of PHC piles under reverse cyclic loading and a constant axial load, and noted that the deformation capacity was improved with a larger stirrup ratio but also affected by the axial load and the ratio of the pile wall thickness to the diameter. Akiyama *et al*. (2012) conducted the flexural tests of precast high-strength reinforced concrete piles with carbon-fibre sheets and concrete infilling, and demonstrated that carbon-fibre sheets and concrete infilling significantly enhanced the flexural capacity of prestressed reinforced concrete piles. The effect of additional non-prestressing reinforcing bars has also been studied by many researchers. Ikeda *et al*. (1982) reported that the non-prestressing longitudinal reinforcements could allow the ductile performance of prestressed concrete piles to develop even after rupture of prestressing tendons. Wu *et al*. (2020) also showed that the failure mode of PHC piles with hybrid glass fibre reinforced polymer (GFRP) bars was gradual crushing of the concrete and a high degree of deformability was attained before failure. Moreover, Yang *et al*. (2018a,

5

1   2018b) investigated the influence of deformed steel bars and concrete infilling on the seismic

2   performance of PHC piles, and pointed out that both methods could enhance the bearing capacity of

3   PHC piles while the use of deformed steel bars could also significantly improve the ductility capacity.

4   Researchers have also investigated the effects of adding steel fibre and using FRP layer to improve

5   the strength and ductility of reinforced concrete (RC) piles. Buyle-Bodin and Madhkhan (2002) noted

6   that steel fibre reinforced concrete (SFRC) piles were as efficient as RC piles in terms of strength and

7   ductility and more efficient in terms of dissipation of energy with axial load. Özden and Akdag (2009,

8   2013) studied the lateral load response of SFRC piles in soil and showed that steel fibres improved

9   the horizontal bearing capacity and ductility of RC piles effectively. In recent years, fibres reinforced

10   polymer (FRP) jacketing has become popular in retrofitting existing deficient piles due to light weight,

11   high strength and excellent corrosion resistance of FRP material. Lignola *et al*. (2017) tested the

12   performance of RC hollow columns with carbon fibre reinforced polymer (CFRP) wraps subjected to

13   combined axial load and bending, and found that the FRP jacketing increased the ultimate load and

14   ductility of hollow columns. Moreover, Murugan *et al*. (2017) pointed out that both GFRP and CFRP

15   confined piles showed higher lateral bearing capacity than unconfined piles, and piles with fibres

16   oriented along the length had higher strength than along the circumference.

17   The above strengthening measures can improve the lateral load capacity and deformation capacity

18   of PHC piles effectively, but they inevitably involve the use of additional materials, a more complex

19   manufacture process and therefore significantly increased costs. As a matter of fact, some

20   experimental results (Ikeda *et al*., 1982; Yang *et al*., 2018a, 2018b) have shown that the brittle failure

21   of PHC piles subjected to lateral load was mainly due to the rupture of prestressing tendons.

22   Muguruma *et al*. (1987) reported that using prestressing tendons with high elongation capacity could

6

1   effectively improve the flexural capacity of PHC piles. Considering that the tensile deformation

2   capacity of prestressing steel bars which are now widely used in PHC piles is not good enough, the

3   present study adopts higher elongation and higher strength prestressing steel strands to replace the

4   prestressing steel bars, and develops pretensioned centrifugal spun concrete piles with steel strands.

5   ## 2. Pretensioned centrifugal spun concrete piles with steel strands

6   The prestressing tendons used in conventional PHC piles are mainly steel bars for prestressed

7   concrete (10G409, 2010). However, the elongation of prestressing steel bars is usually not good

8   enough and sometimes they show brittle fracture, which limits the deformation capacity of PHC piles

9   when subjected to lateral load. Moreover, all steel bars are fixed on the end plates (an anchoring plate

10   and a tensioning plate) of a pile with pier heads that cannot be in full contact with the plates during

11   tensioning, which leads to uneven stresses in the prestressing steel bars and affects the bearing

12   capacity of PHC piles. Therefore, changing the material of prestressing tendons and improving the

13   manufacture process are deemed to be a viable approach to enhance the horizontal bearing capacity

14   and deformation capacity of PHC piles.

15   Steel strand is a common type of prestressing tendons with high tensile strength and good tensile

16   ductility, and is used in precast and prestressed concrete structures (Park *et al*., 2016; Paul *et al*., 2017;

17   Dang *et al*., 2018). In pile foundations, particularly in solid square and octagonal prestressed concrete

18   piles, prestressing strands are also widely used (PCI, 2017). The post-tensioned hollow pipe piles,

19   which were first manufactured by the American Raymond Pile Company, were popular in port

20   engineering due to large modulus and relatively light section. However, because of the post-tensioned

21   method, a large cross-section diameter is required, and consequently the cost is also high, making it

22   uneconomical to use post-tensioned hollow pipe piles in pile foundation engineering of high-rise

7

1 buildings.

2   In the present study, a new pretensioned centrifugal spun concrete pile with steel strands is

3   developed to combine the excellent mechanical properties of prestressing strands with the advantages

4   from the well-developed technology of pretensioned spun concrete piles. Comparing to the steel bars,

5   it is more difficult to fully fix the steel strands, which are made up by a plurality of steel wires, to end

6   plates. Therefore, a new design of the end plate with an improved anchorage method has been

7   developed for the prestressing tendons (Yu and Gao, 2016; Gan *et al*., 2017). The end plate has a

8   plurality of conical through holes, and the diameter of the holes is made to gradually increase from

9   inside towards outside and each hole hosts one individual steel strand, as depicted in Figure 1. A

10 chock assembly constituted of multiple metal clips with a toothed inner surface and a conical outer

11 surface is placed in each hole. The steel strand passes through a corresponding chock assembly and

12 is clamped tightly on the end plate. Following a series of preliminary studies and continuous

13 improvements, a reliable manufacture process of pretensioned centrifugal spun concrete piles with

14 steel strands has been established. In order to examine the flexural performance of the new pile,

15 bending tests on full-scale pile test specimens were carried out.

16 ## 3. Experimental programme

17 3.1 Detail of test specimens

18   Full-scale bending tests of six pile test specimens were carried out. According to the size of PHC

19 piles commonly used in practical engineering, the test piles had external diameters of 400 mm, 500

20 mm and 600 mm, respectively. For a comparison, each diameter group consisted of two piles, namely

21 an ordinary pretensioned spun high strength concrete pile with prestressing steel bars (PHC pile) and

22 a pretensioned spun high strength concrete pile with prestressing steel strands (PSC pile). Figure 2

8

1   and Table 1 show the details of these piles. The three PHC pile test specimens are labelled as PHC400,

2   PHC500 and PHC600, and their counterpart PSC pile test specimens as PSC400, PSC500, and

3   PSC600, respectively.

4   The only difference between the two types of piles in each diameter group was the type of

5   prestressing tendons. The steel bars used in PHC piles were 10.7 mm in diameter (cross-section area

6   = 90 mm^2) and they had a nominal tensile strength of 1420 MPa. The nominal strength of the steel

7   strands in PSC piles was higher at 1860 MPa. Because the control stresses for pretensioning of steel

8   bars and steel strands were kept at 70% of the nominal tensile strength in both PHC and PSC piles,

9   7-wire steel strand of nominal diameter of 11.1 mm, which has a smaller net cross-section area of

10   74.2 mm^2, was selected to ensure the effective compressive pre-stress of concrete was comparable

11   between PHC and PSC piles. For the same reason, the load-carrying capacity of the steel bars and the

12   steel strands between PHC and PSC piles was also similar.

13   3.2 Material mechanical properties

14   The design strength grade of the concrete for the pile test specimens was C105. The concrete was

15   mixed with a mass ratio of cement, water, sand and gravel as 1.00 : 0.26 : 1.12 : 2.60. In order to

16   obtain the material parameters of high-strength concrete, nine concrete cubes of size 100 mm were

17   prepared in the same curing condition as the pile test specimens for compressive tests. The average

18   value of the cubic compressive strength $f_{cu,10}$ was found to be 116.1 MPa. The standard cubic

19   compressive strength f_{cu}, axial compressive strength f_c and tensile strength f_t of the concrete material

20   may be estimated using the empirical formulas for high strength concrete such as the following (Li,

21   2004; Ke, 2014):

22   1. $$f_{cu} = 0.91 f_{cu,10} + 1$$

9

1   2. $f_c = 0.818 f_{cu}$

2   3. $f_t = 0.26 f_{cu}^{2/3}$

3   The test piles used low relaxation helical grooved steel bars and steel strands as prestressing

4   tendons, and grade-A cold drawn low carbon steel wires as spiral stirrups. Three samples were taken

5   from each type of reinforcing bars, including $\Phi^D 10.7$ steel bars, $\Phi^S 11.1$ steel strands and $\Phi^b 6$ steel

6   wires for the stirrups, and tested to measure the tensile properties. It should be noted that due to the

7   difficulty to hold $\Phi^b 4$ and $\Phi^b 5$ steel wires in the standard tensile testing machine, three samples of

8   $\Phi^b 6$ (6 mm in diameter) from the same type wires were tested instead. Figure 3 shows the measured

9   stress-strain curves, and Table 2 lists the critical material mechanical parameters of three types of

10 reinforcing bars. It can be observed that the ultimate tensile strength f_u and maximum elongation δ of

11 steel strands are much higher than those of helical grooved steel bars.

12 3.3 Test setup and loading schedule

13   The bending experiments of the pile test specimens were carried out mainly to investigate the

14 flexural performance of the piles. According to the pretensioned spun concrete piles standard (GB

15 13476-2009, 2009), the 4-point loading scheme was adopted in the experiments, and the load was

16 applied using an electro-hydraulic servo multi-functional testing machine controlled by a computer,

17 as shown in Figure 4(a). Five displacement transducers were installed to measure the displacements

18 at the middle and quarter-span points, as well as at two support locations to monitor any support

19 settlements. Nine concrete strain gauges were installed to monitor the distribution of the strain over

20 the depth of the midspan cross-section and along the bottom tensile edge at locations close to the

21 midspan.

22   The loading was terminated when rupture of prestressing tendons in the tension zone or crushing

10

1 of concrete in compression zone occurred. As shown in Figure 4(b), each pile test specimen was 8.0

2 m long in total, and had a net test length of 4.8 m between two supports with a 1.0 m pure bending

3 segment in the midspan. Thus, the bending moment in the midspan of pile test specimens is given by:

4 4. $$M_\mathrm{e} = \frac{P}{4}\left(\frac{3}{5}L - 1\right) + \frac{1}{40}WL$$

5 where P is the total load applied via the testing machine; L and W are the length and the self-weight

6 of test specimens, respectively.

7 The cracking moment M_cr and the ultimate bending moment M_u of pile test specimens were first

8 estimated according to the relevant standard (10G409, 2010). The loading scheme was then stipulated

9 accordingly, as follows. Firstly, the load was applied at a 20% increment of M_cr, until the bending

10 moment in the midspan segment reached 80% of M_cr. Subsequently, a smaller load increment was

11 applied until the actual cracking of the concrete. After the first vertical crack appeared, a 5%

12 increment of M_u was applied until the bending moment in the midspan segment reached M_u.

13 Afterwards, the loading was changed to the displacement control with a displacement increment of 2

14 mm until the failure of test specimens. Each loading step was maintained about 3 minutes for the

15 stabilization of the test specimens and measurement readings.

16 **4. Experimental results and analysis**

17 4.1 Load-deflexion curves

18 Figure 5 shows the load-deflexion curves in the midspan of the six pile test specimens. The

19 cracking and maximum load points are marked in the diagrams, and the black and red lines represent

20 the PHC and PSC piles, respectively.

21 Combining the experimental phenomena with the load-deflexion curves, the entire loading process

22 may be described by three distinctive stages: 1) At the first stage of loading, each pile test specimen

11

1 exhibited an elastic behaviour and the load increased linearly with the midspan deflexion. The

2 bending stiffness of PSC piles was essentially equal to that of PHC piles of the same pile diameter. 2)

3 When the first vertical crack occurred in the midspan, the bending stiffness began to decrease

4 markedly, and the drop of the bending stiffness of PSC piles due to the cracking appeared to be more

5 than that of the corresponding PHC piles, but the degradation rate of the bending stiffness of PSC

6 piles after the cracking was slower as the load further increased. 3) Approaching failure, the steel bar

7 in the bottom of PHC piles went through a hardening phase and eventually reached its ultimate tensile

8 strength and ruptured. The main cracks in the midspan developed greatly in this process, however the

9 concrete in the compression zone of midspan did not crush. In contrast, the failure mode of PSC piles

10 was notably different. The cracks in the midspan appeared gradually with the increase of the deflexion

11 and the bearing capacity of test specimens continued to increase, until the concrete in the compression

12 zone crushed completely. Overall, the PHC piles exhibited a brittle failure mode with the rupture of

13 prestressing tendons, while the PSC piles showed a more ductile failure mode with the compressive

14 concrete eventually crushing but without the rupture of the prestressing strands. Figure 6 shows the

15 representative failure modes of PHC and PSC piles.

16 4.2 Flexural performance

17 Table 3 presents the comparison of flexural performance between PHC and PSC pile test specimens.

18 It can be observed that on average there is little difference in the cracking moment $M_{cr,e}$ between the

19 corresponding PHC and PSC piles of the same diameter. However, the difference of cracking moment

20 between PHC400 and PSC400 pile specimens is relatively large, which may be ascribed to

21 insufficient initial pre-stress of PSC400 pile specimen. Additionally, the ultimate bending moment

22 $M_{u,e}$ of PSC piles were 7%, 17% and 11% larger than that of the corresponding PHC piles, respectively.

12

1   Notably, the maximum midspan deflexions $f_{u,e}$ corresponding to the maximum load of PSC piles

2   were 20%, 50% and 26% greater than their respective PHC counterparts. This indicates that using the

3   steel strands instead of the steel bars as the prestressing tendons has significantly improved the

4   deformation capacity of the piles.

5   4.3 Crack distribution

6   Figure 7 shows the crack distribution of six pile test specimens before complete failure. The

7   following observations may be made: 1) In both PHC and PSC piles, the crack distributions were

8   generally uniform, and the crack extension height and distribution ranges were similar between PHC

9   and PSC piles. 2) For the two types of piles, with the increase of the pile diameter, the number of

10   cracks increased and the maximum crack width decreased. 3) When the failure of PHC piles occurred

11   in the midspan, the prestressing steel bar in the bottom tension zone ruptured and the width of the

12   main crack increased sharply. On the other hand, the failure of PSC piles was due to the crushing of

13   the concrete in the compression zone, which resulted in the bifurcation of vertical cracks in the

14   midspan.

15   4.4 Strain development

16   As described in Section 3.3, concrete strain gauges were installed on the surface of the piles to

17   measure the strain of concrete at selected critical locations, mainly for the purpose to monitor the

18   occurrence of initial cracking, as well as the crack extension along the depth of the midspan section.

19   The strain histories as measured from these strain gauges are plotted against the applied load in Figure

20   8, in which the cracking and maximum loads are represented by two vertical lines. Note that the

21   tensile strain data above 1500 $\mu\varepsilon$ are deemed to be meaningless due to cracking and therefore are

22   omitted in the figures. It can be observed that before the cracking in the midspan, the strain from each

13

1   strain gauge was small and increased linearly with the load. There was an abrupt increase in some

2   tensile strain gauges near the initiation of cracking. When the first crack appeared, the strain in the

3   tension zone increased rapidly and some strain gauges failed just after the cracking.

4   Figure 9 shows the strain distribution over the depth of the midspan section. It can be observed that

5   the concrete strain in the midspan section basically conformed to the assumption of plane section

6   before the cracking. After the cracking and with the load increasing, the neutral axis of the cross-

7   section moved upward continuously.

8   The initial concrete strain of each test specimen before applying external loading was not available

9   but it may be estimated based on the effective compressive pre-stress and the elastic modulus of

10   concrete. Adding the so calculated initial strain values to the maximum readings of concrete strain

11   gauges in the compression zone, the maximum compressive strain of the concrete for all test

12   specimens can be obtained. The average values are found to be about 2300 $\mu\varepsilon$ in PHC piles and 2800

13   $\mu\varepsilon$ in PSC piles. These values tend to suggest that the compressive performance of the high strength

14   concrete was better attained in PSC piles as compared to PHC piles, possibly because of an improved

15   interaction between the prestressing strands and concrete as compared to the more rigid prestressing

16   steel bars.

17   **5. Theoretical analysis of flexural strength**

18   This section presents a theoretical analysis of the flexural strength of the pile test specimens. The

19   flexural strength of prestressed circular hollow section piles is affected by several inter-connected

20   factors such as the prestressing level and the circular arrangement of the reinforcements, therefore

21   the theoretical analysis is not straightforward. The present experiments on full-scale pile test

22   specimens provide a unique opportunity to verify the accuracy of theoretical calculations concerning

14

1   the flexural strength. The theoretical analysis is carried out at a cross-section level and is based on

2   the strain compatibility, force equilibrium, and constitutive relationships for the reinforcing bars and

3   the concrete.

4   5.1 General calculation method

5   Similar to the calculation of the bearing capacity of ordinary flexural members, it is assumed that

6   a cross-section of piles remains plane at all loading stages and perfect bonding exists between the

7   prestressing tendons and the concrete (Qiao *et al*., 2018). However, the analysis of an annular section

8   is much more complicated than rectangular section and the prestressing tendons are distributed in a

9   circle, which requires to a more sophisticated calculation. Referring to the recommendations in the

10   literature (Joen and Park, 1990; GB 50010-2010, 2010), herein the pile cross-section is divided into

11   a number of discrete strips, as shown in Figure 10, and each strip is calculated as an approximate

12   rectangle and the stress within a strip is assumed to be constant.

13   To calculate the theoretical ultimate bending moment, the maximum compressive strain of concrete

14   in the current PHC and PSC piles is assumed to be 2300 $\mu\varepsilon$ and 2800 $\mu\varepsilon$, respectively, based on the

15   experimental data as mentioned in Section 4.4. The calculation procedure is summarized into the

16   following steps (Qiao *et al*., 2018):

17   1. Select appropriate constitutive relationships of concrete and prestressing tendons, and determine

18   the initial strain of concrete and prestressing tendons. Details will be described in Section 5.2.

19   2. Assume an initial value for the neutral axis depth h.

20   3. According to the difference between the maximum compressive strain and the initial strain of

21   concrete in the upper edge strip and the plane section assumption, the strain increments of concrete

22   in the other strips are calculated, and subsequently the strain and the stress are obtained. The

15

compressive force of concrete F_c can be determined as follows:

5. $$F_c = \sum_{i=1}^{n_c} f_{ci} A_{ci}$$

where f_{ci} is the stress in the i-th concrete strip (positive if compression); A_{ci} is the area of the i-th

concrete strip.

4. Based on the assumption that perfect bonding exists between the prestressing tendons and the

concrete, the strain of prestressing tendons is comprised of the initial strain and strain increment

which is assumed to be the same as that of surrounding concrete. The stress of the prestressing tendons

is then calculated from the constitutive relationship, and from there the tensile force of prestressing

tendons F_p can be determined as follows:

6. $$F_p = \sum_{j=1}^{n_p} f_{pj} A_{pj}$$

where f_{pj} is the stress in the j-th prestressing tendon (positive if compression); A_{pj} is the area of the j-

th prestressing tendon.

5. Check the force equilibrium of section by satisfying that the absolute value of the sum of

compressive force F_c and tensile force F_p is less than a certain allowable tolerance ζ.

7. $$\left| F_c + F_p \right| \le \zeta$$

6. If the force equilibrium is not satisfied, revise the value h and repeat from step 2 until the force

equilibrium is achieved.

7. When force equilibrium is satisfied, the section bending moment M can be determined as follows:

8. $$M = \sum_{i=1}^{n_c} f_{ci} A_{ci} y_{ci} + \sum_{j=1}^{n_p} f_{pj} A_{pj} y_{pj}$$

where y_{ci} is the distance from the centroid of the i-th concrete strip to the central axis of the pile

section; y_{pj} is the distance from the centroid of the j-th prestressing tendon to the central axis of the

16

1   pile section.

2   5.2 Constitutive relationships

3   In the above calculations, the constitutive relationships of concrete and prestressing tendons are

4   needed. There are many stress-strain relationships for concrete in the literature, and the material

5   model proposed by Velasco (2008) about uniaxial compression and tension stress-strain curves is

6   adopted herein for the constitutive relationship of the high strength concrete.

7   The uniaxial compression stress-strain curve of concrete is composed by three sections: initial

8   elastic section, damage-based plastic rising section and damage-based plastic descending section, as

9   illustrated in Figure 11(a). The constitutive relationship is given by the following equations:

10   9.
$$
\sigma_c = \begin{cases}
E_c \varepsilon_c & \varepsilon_c \in [0, \varepsilon_{c0}] \\[2em]
\sigma_{cm}\left[1 - \left(1 - \dfrac{\varepsilon_c}{\varepsilon_{cm}}\right)^{\eta_1}\right] & \varepsilon_c \in (\varepsilon_{c0}, \varepsilon_{cm}] \\[2em]
\sigma_{cm}\left[1 - \left(\dfrac{\varepsilon_c - \varepsilon_{cm}}{\varepsilon_{cf} - \varepsilon_{cm}}\right)^{\eta_2}\right] & \varepsilon_c \in (\varepsilon_{cm}, \varepsilon_{cf}]
\end{cases}
$$

11   where E_c is the elastic modulus of concrete and can be calculated by $E_c = 10200 f_c^{1/3}$ (Wee *et al.*,

12   1996); σ_{cm} is the peak compressive stress, which is taken as equal to the axial compressive strength

13   of concrete; ε_{c0} is the elastic compressive strain, the value is 0.001; ε_{cm} is the peak compressive strain

14   and can be calculated by $\varepsilon_{cm} = 0.00078 f_c^{1/4}$ (Wee *et al.*, 1996); ε_{cf} is the final compressive strain, the

15   value is taken as 0.0045 based on the compression test; η_1 and η_2 are the empirical parameters related

16   to smoothness of the curve, the values are 1.434 and 1.650, respectively.

17   The uniaxial tension stress-strain curve of concrete can be described by a piece-wise linear line

18   consisting of four segments, as shown in Figure 11(b). The rising section of the curve is a linear elastic

17

1   section and the descending section of the curve is composed by three segments, passing through three

2   points $(\varepsilon_{t1}, \sigma_{t1})$, $(\varepsilon_{t2}, \sigma_{t2})$, $(\varepsilon_{tf}, 0)$ in turn. The coordinates of the controlling points are obtained by the

3   following expressions: $\sigma_{t1} = b_1 \sigma_{tm}$, $\sigma_{t2} = b_2 \sigma_{tm}$, $\varepsilon_{t1} = (\varepsilon_{tf} - \varepsilon_{tm})/c_1$, $\varepsilon_{t2} = (\varepsilon_{tf} - \varepsilon_{tm})/c_2$, and

4   the constitutive relationship is given by the following equations:

5   10.
$$\sigma_t = \begin{cases} E_c \varepsilon_t & \varepsilon_t \in [0, \varepsilon_{tm}] \\[2mm] \dfrac{\sigma_{tm} - \sigma_{t1}}{\varepsilon_{tm} - \varepsilon_{t1}}(\varepsilon_t - \varepsilon_{tm}) + \sigma_{tm} & \varepsilon_t \in (\varepsilon_{tm}, \varepsilon_{t1}] \\[3mm] \dfrac{\sigma_{t1} - \sigma_{t2}}{\varepsilon_{t1} - \varepsilon_{t2}}(\varepsilon_t - \varepsilon_{t1}) + \sigma_{t1} & \varepsilon_t \in (\varepsilon_{t1}, \varepsilon_{t2}] \\[3mm] \dfrac{\sigma_{t2}}{\varepsilon_{t2} - \varepsilon_{tf}}(\varepsilon_t - \varepsilon_{tf}) & \varepsilon_t \in (\varepsilon_{t2}, \varepsilon_{tf}] \end{cases}$$

6   where σ_{tm} is the peak tensile stress, which is taken as equal to the tensile strength of concrete; ε_{tm} and

7   ε_{tf} are the peak tensile strain and the final tensile strain, respectively; b_1 and b_2 are the empirical

8   parameters that can better describe the softening behaviour in uniaxial tension test, the values are 0.33

9   and 0.1, respectively; c_1 and c_2 are the constants, and the values are 10 and 1.5, respectively.

10   As shown earlier in Figure 3, the shapes of the stress-strain curves of the prestressing steel bar and

11   prestressing strand are similar, and both exhibit a linear elastic stage that is followed immediately by

12   a hardening stage, without obvious yield plateau. Therefore, the model proposed by Esmaeily and

13   Xiao (2005) is adopted to describe the stress-strain curve, as shown in Figure 12, according to the

14   following expressions:

15   11.
$$\sigma = \begin{cases} E_s \varepsilon & \varepsilon \in [0, \varepsilon_y] \\[3mm] k_3 f_y + \dfrac{E_s(1 - k_3)}{\varepsilon_y (k_1 - 1)^2}(\varepsilon - k_1 \varepsilon_y)^2 & \varepsilon \in (\varepsilon_y, k_2 \varepsilon_y] \end{cases}$$

16   where E_s and ε_y are the elastic modulus and the yield strain of reinforcing bars respectively, which

18

1   are obtained from the tensile test; k_1 is the ratio of the peak strain to the yield strain, k_2 is the ratio of

2   the ultimate strain to the yield strain, and k_3 is the ratio of the peak stress to the yield stress.

3   5.3 Simplified calculation method

4   The general calculation method described in Section 5.1 requires iteration and so needs to be

5   implemented through a computer programme. For practical calculations, a further simplified

6   formulation is proposed in this section, using an arc analogy with a polar coordinate system. For a

7   simple calculation of the area of the concrete in the compression zone, it is assumed that the

8   compression zone is distributed as an annular segment, as shown in Figure 13, and the equivalent

9   height of compression zone concrete is taken as the average value of the heights of the outer arc and

10   the inner arc (Zhang *et al*., 2019). In addition, a thin steel arc is used to replace the discrete

11   prestressing tendons, and through the total steel area equivalence the wall thickness of the arc can be

12   found as $\delta_p = A_p / 2\pi r_p$.

13   The distribution of the stresses in the prestressing strands at the ultimate state under bending is

14   complicated. For simplicity and by reference to the numerical results using the finite element

15   simulation as will be described in section 6.3, it is assumed that at the ultimate state the stress

16   distributions of the prestressing tendons in the upper and lower parts of the pile cross-section

17   (bounded by the central axis) are both linear, as shown in Figure 13. The stress of the prestressing

18   tendon at the central axis reaches the yield strength, and the stress of the bottom prestressing tendon

19   reaches the ultimate tensile strength.

20   According to the geometric relationship shown in Figure 13, the depth of the equivalent concrete

21   compression zone h_e and the depth of neutral axis h can be calculated as follows:

22   12. $h_e = r_1 - r_c \cos\pi\alpha$

19

1   13. $$h = h_e / \beta_1$$

2   where r_c is the average radius of the cross-section. The value of r_c should be very close to the radius

3   r_p of the circle along which the prestressing tendons are distributed, and for simplicity take $r_c = r_p$. β_1

4   is the ratio of the depth of equivalent rectangular stress block to the depth of neutral axis, the value

5   can be taken as 0.65 (ACI, 2019).

6   Above the central axis, the stress of prestressing tendons σ at any height y can be calculated as

7   follows:

8   14. $$\sigma = \frac{r_1 - h - y}{r_1 - h}\left(f_y - \sigma_{p0}\right) + \sigma_{p0}$$

9   where f_y is the yield strength of prestressing tendons; σ_{p0} is the initial stress of prestressing tendons.

10   The stress of prestressing tendons below the central axis can be calculated as follows:

11   15. $$\sigma = f_y - \frac{y}{r_p}\left(f_{pt} - f_y\right)$$

12   where f_{pt} is the tensile strength of prestressing tendons.

13   The tensile force of the prestressing tendons F_p can be calculated as:

14   16. $$F_p = 2\int_{-\pi/2}^{\pi/2} \sigma \delta_p r_p \, d\theta = \frac{f_{pt} - f_y}{\pi} A_p - \frac{\beta_1 r_p \left(f_y - \sigma_{p0}\right)}{\pi\left[(\beta_1 - 1)r_1 + r_p \cos\pi\alpha\right]} A_p + f_y A_p$$

15   On the other hand, the compressive force of concrete F_c can be calculated as:

16   17. $$F_c = \alpha_1 \alpha A f_c$$

17   where α_1 is the ratio of stress of equivalent rectangular concrete block in the compression zone to

18   axial compressive strength of concrete, the value can be taken as 0.85 (ACI, 2019); A is the cross-

19   section area of the pile.

20   Based on the axial force equilibrium, the value of α can be obtained by an iterative calculation to

21   satisfy:

20

1   18.

$$\alpha_1 \alpha A f_c = \frac{f_{pt} - f_y}{\pi} A_p - \frac{\beta_1 r_p \left(f_y - \sigma_{p0} \right)}{\pi \left[(\beta_1 - 1) r_1 + r_p \cos \pi \alpha \right]} A_p + f_y A_p$$

2   The total bending moment of the section is the sum of the moments produced by the compression

3   zone concrete and the tensile prestressing tendons, which can be obtained by multiplying F_c and F_p

4   by their respective distances to the central axis x. Then the resultant (total) moment can be calculated

5   as follows:

6   19.

$$M = \alpha_1 f_c \int_{\pi/2-\pi\alpha}^{\pi/2+\pi\alpha} r_c \sin\theta \frac{A}{2\pi} d\theta + 2 \int_{-\pi/2}^{\pi/2} -\sigma \delta_p r_p d\theta r_p \sin\theta$$

$$= \alpha_1 A f_c \frac{\sin\pi\alpha}{\pi} r_p + \frac{\left(f_{pt} - f_y \right) r_p A_p}{4} + \frac{\left(f_y - \sigma_{p0} \right) \beta_1 r_p^2 A_p}{4 \left[(\beta_1 - 1) r_1 + r_p \cos\pi\alpha \right]}$$

7   5.4 Theoretical bending moment capacities and comparison with experimental results

8   The bending moment strengths for the pile test specimens are calculated using both the general

9   method described in Section 5.1 and the simplified method in Section 5.3, and the results are

10 compared with the experimental results in Table 4. Note that h_g and h_s in the table denote the depth

11 of the neutral axis of the cross-section obtained by the two methods, respectively. It can be observed

12 that the bending moment capacities and the depth of neutral axis calculated using the general and

13 simplified methods match closely with each other, indicating that the simplification using the arc

14 analogy is effective. The two groups of calculated values compare reasonably well with the

15 experimental results; however, the predicted values are generally lower than the experimental results

16 by a margin of less than 15%.

17 The above comparisons indicate that the two calculation methods can predict the flexural capacity

18 of the pile test specimens with reasonable accuracy, and therefore may be used to evaluate the flexural

19 strength of prestressed concrete piles in practical applications.

21

6. Finite element analysis

Using the above theoretical methods, the bending strength of different type of prestressed concrete piles can be estimated with reasonable accuracy. In order to assist in further evaluation of the damage process and facilitate the parametric investigations, a finite element model has been developed for prestressed concrete piles and verified against the experimental results.

6.1 Finite element model

The finite element analysis is carried out using the software ABAQUS to simulate the flexural performance of the pile test specimens. Figure 14 shows the configuration of the finite element model. The geometric dimensions and loading condition of the model are the same as the experiments. In order to avoid artificial stress concentration and numerical singularity at the loading points, two elastic loading blocks similar to the experiments are added onto the pile model. An eight-node three-dimensional solid element with reduced integration (C3D8R) is chosen for concrete and a two-node three-dimensional truss element (T3D2) is used for reinforcing bars which are embedded into the concrete. The initial pre-stress of the concrete is applied with an equivalent method of decreasing the temperature of prestressing tendons. In order to ensure the convergence of the solution process, the displacement loading is adopted.

On the basis of sensitivity analysis of mesh size, the cross-section of the pile models is meshed into 4 layers through the thickness and 36 divisions in the circumferential direction. In the length direction, the mesh density gradually becomes coarser from the midspan segment to two sides of overhanging segments, and the mesh length in the pure bending part is 25 mm, as shown in Figure 14.

6.2 Material parameters

The concrete damage plasticity (CDP) model in ABAQUS is used for the high strength concrete.

22

1   The CDP model is based on isotropic damage combined with isotropic tensile and compressive

2   plasticity to describe the inelastic behaviour of concrete, which can simulate the cumulative damage

3   in concrete. The uniaxial compression and tension stress-strain curves mentioned in Section 5.2 are

4   employed to define the constitutive relationships of the high strength concrete under consideration.

5   Other parameters of CDP model are determined by referring to relevant studies (An *et al*., 2012;

6   Genikomsou and Polak, 2015; Yilmaz *et al*., 2019) and trial calculations as follows: dilation angle ψ

7    $= 45°$, eccentricity $\in = 0.1$, $\sigma_{bo} / \sigma_{co} = 1.16$, $K = 0.6667$, and viscosity parameter $\mu = 0.001$.

8   The mechanical properties of reinforcing bars are modeled by the standard plastic model, and a

9   thermal expansion coefficient is defined to generate the initial pre-stress of the concrete resulting

10   from the initial prestressing condition. The stress-strain relationship for reinforcing bars mentioned

11   in Section 5.2 is adopted to define the basic constitutive properties. The detailed parameter values of

12   reinforcing bars are shown in Table 5.

13   6.3 Numerical results

14   Using the above finite element model, numerical simulations of PHC and PSC piles have been

15   performed. Figure 15 shows the comparison of the load-deflexion curves between the numerical and

16   experimental results. It should be noted that for PHC piles, the failure limit is considered to have been

17   reached when the tensile strain of the prestressing steel bar in the lowest layer reaches the

18   experimental rupture strain of 0.034. It can be observed that the simulated curves match closely the

19   experimental curves before the cracking, and show good agreement after the cracking and throughout

20   the inelastic response range.

21   A comparison of the flexural performance parameters of the pile test specimens between numerical

22   and experimental results is shown in Table 6. It can be seen that the cracking bending moment $M_{cr,n}$

23

1 obtained by the numerical simulation are in good agreement with the experimental results besides the

2 pile specimen PSC400 due to insufficient initial pre-stress. In addition, the simulated values of

3 ultimate bending moment $M_{u,n}$ for all pile specimens are generally lower but within a margin of 10%.

4 The deflexions obtained from the numerical simulation are also consistent with the experimental

5 results, but the margin of errors is slightly larger than that for the bending strength. These comparisons

6 suggest that the finite element modelling scheme used in this analysis is adequate for the evaluation

7 of the flexural performance of PHC and PSC piles.

8 The finite element simulation allows a detailed examination of the strain distribution in the

9 prestressing tendons. Figure 16 shows the strain distribution of the prestressing tendons in the

10 midspan section at some key loading stages, including concrete cracking, yield of prestressing

11 tendons at different depths of the cross-section, and finial failure. The yield sequence shown in Figure

12 16 corresponds to the yield of prestressing tendons layer by layer from the bottom to the top. The

13 arrangement of prestressing tendons in the pile cross-section is shown in Figure 17.

14 It can be observed that before the yield of the bottom prestressing tendon, the strain of prestressing

15 tendons is linearly distributed over the depth of the cross-section, which satisfies the assumption of

16 plane section. With the cracking of concrete and yielding of the prestressing tendons from the bottom

17 layer, the increase of strain in the lower prestressing tendons (i.e. the flexural tension side) accelerates.

18 The strain distribution may still be regarded as following approximately a linear distribution, until

19 the prestressing tendons below the central axis of the section all reach yield strength. After about half

20 of the prestressing tendons in the cross-section have yielded, the strain of prestressing tendons below

21 the central axis increases significantly, suggesting that the assumption of plane section is no longer

22 applicable.

24

1   Figure 17 shows the stress distribution of prestressing tendons at the failure stage. It can be found

2   that the stress distribution of prestressing tendons over the depth of the cross-section is approximately

3   a two-fold linear distribution. The turning point is above the central axis of the cross-section, and the

4   stress at this point is close to the yield strength. The stresses of the prestressing tendons at and below

5   the central axis all exceed the yield strength, and the stress of the prestressing tendon at the lowest

6   layer approaches the ultimate tensile strength.

7   From the finite element results, the crack distribution of concrete can be observed by the maximum

8   principal plastic strain. In the CDP model, it is assumed that the cracking occurs when the maximum

9   principal plastic strain of concrete is positive and the crack direction is perpendicular to the maximum

10   principal plastic strain (Genikomsou and Polak, 2015). Figure 18 shows the comparison of crack

11   distribution in the pile when the ultimate bending moment is reached between numerical and

12   experiment results. As can be seen, the patterns of the cracks from the numerical model generally

13   resemble the crack distribution from the experimental results.

7. Conclusions

15   A new type of pretensioned spun concrete piles with high strength and high elongation steel strands

16   has been developed for use in high intensity seismic areas. To evaluate the flexural performance of

17   the new type of piles, bending tests have been conducted on six full-size pile test specimens with

18   three different cross-section diameters. In conjunction with the experiments, theoretical analysis and

19   finite element modelling of the pile test specimens have also been carried out. The differences in the

20   crack resistance, flexural capacity, deformation capacity and failure mode between the PHC and PSC

21   piles are compared and analyzed. The main conclusions can be summarized as follows:

22   1. With the use of high strength and high elongation prestressing strands instead of prestressing steel

25

1   bars as longitudinal reinforcements, the new PSC piles achieved significant improvement in the

2   lateral deformation capacity. The special end plate design ensured sufficient anchorage and a

3   uniform pre-stress distribution of steel strands in the piles.

4   2. Because a higher tensile control stress with the use of prestressing strands, less longitudinal

5   reinforcement ratio can achieve the same effective compressive pre-stress of concrete. In the pile

6   test specimens, the quantity of longitudinal reinforcement of PSC piles was about 17.6% lower

7   than that of PHC piles of the same cross-section diameter. The experimental cracking moments

8   of the PSC piles were similar to those of the corresponding PHC piles, and the ultimate bending

9   moments of the PSC piles were on average about 11% larger than those of the PHC piles. The

10   new PSC piles exhibited comparatively better flexural capacity.

11   3. The new PSC piles showed markedly increased deformation capacity comparing to their

12   traditional PHC counterparts. The maximum midspan deflexions of the PSC pile test specimens

13   were observed to increase by 20%, 50% and 26% from those of the corresponding PHC pile test

14   specimens, respectively.

15   4. The failure mode of the PHC pile test specimens was brittle bending failure with the rupture of

16   prestressing steel bars, while the failure mode of PSC pile test specimens was governed by the

17   eventual crushing of concrete in the compression zone, without rupture of prestressing strands.

18   The failure process of the PSC piles was more gradual and it exhibited the characteristic of ductile

19   failure, indicating that the PSC piles can be suitable in seismic areas.

20   5. The theoretical method is able to predict the flexural strength of prestressed concrete piles

21   reasonably well. The predicted values tend to be slightly lower, and hence on the conservative

22   side, than the experimental results by a margin of less than 15%. The simplified version of the

26

1   method enables hand calculations and is therefore convenient for practical application.

2   6. Using a general-purpose finite element approach (with ABAQUS herein), the behaviour of the

3   prestressed concrete piles can be simulated satisfactorily. The simulated load-deflexion curves

4   compare well with the experimental curves, including key stages of cracking, maximum bending

5   moment and ultimate midspan deflexion. The finite element model also can capture the strain

6   distribution of prestressing tendons in the midspan section at any critical moment and the

7   development of cracks in the piles through the plastic strain distribution.

8   In future research, more parametric studies may be conducted to cover a wider range of design

9   parameters for the PSC piles, and the parametric study can be assisted by the finite element model as

10   verified in the present paper. Furthermore, for the general application of PSC piles in seismic regions,

11   the behaviour of PSC piles under combined bending and shear, as well as lateral and axial loading,

12   will need to be evaluated. Studies in this direction are underway and the results will be reported

13   subsequently.

14   **Acknowledgement**

18   **REFERENCES**

19   10G409 (2010) Prestressed concrete pipe piles. China Planning Press, Beijing.

20   ACI (2019) Building code requirements for structural concrete (ACI 318-19). American Concrete

21   Institute, Farmington Hills, MI.

22   Akdag CT and Özden G (2013) Nonlinear behavior of reinforced concrete (RC) and steel fiber added

27

RC (WS-SFRC) model piles in medium dense sand. *Construction and Building Materials* **48**: 464-472.

Akiyama M, Abe S, Aoki N and Suzuki M (2012) Flexural test of precast high-strength reinforced concrete pile prestressed with unbonded bars arranged at the center of the cross-section. *Engineering Structures* **34**: 259-270.

An C, Castello X, Duan M, Filho RDT and Estefen SF (2012) Ultimate strength behaviour of sandwich pipes filled with steel fiber reinforced concrete. *Ocean Engineering* **55**: 125-135.

Buyle-Bodin F and Madhkhan M (2002) Performance and modelling of steel fibre reinforced piles under seismic loading. *Engineering Structures* **24(8)**: 1049-1056.

Dang CN, Floyd RW, Hale WM and Martí-Vargas JR (2018) Prediction of development length from free-end slip in pretensioned concrete members. *Magazine of Concrete Research* **70(14)**: 714-725.

Esmaeily A and Xiao Y (2005) Behavior of reinforced concrete columns under variable axial loads: analysis. *ACI Structural Journal* **102(5)**: 736-744.

Gan G, Yu XY and Zeng K (2017) Pre-tensioned centrifugal concrete pile provided with steel strands. US9783987(B2).

GB 13476-2009 (2009) Pretensioned spun concrete piles. China Standard Press, Beijing.

GB 50010-2010 (2010) Code for design of concrete structures. China Architecture and Building Press, Beijing.

Genikomsou AS and Polak MA (2015) Finite element analysis of punching shear of concrete slabs using damaged plasticity model in ABAQUS. *Engineering Structures* **98**: 38-48.

Ikeda S, Tsubaki T and Yamaguchi T (1982) Ductility improvement of prestressed concrete piles.

1   *Transactions of the Japan Concrete Institute* **4**: 531-538.

2   Joen PH and Park R (1990) Flexural strength and ductility analysis of spirally reinforced prestressed

3   concrete piles. *PCI Journal* **35(4)**: 64-83.

4   Ke XJ (2014) Study on seismic performance and design method of new high-strength concrete

5   composite columns. PhD Thesis, Xian University of Architecture and Technology, Xian.

6   Kishida S, Horii M, Kuwabara F and Hayashi S (2000) Experimental study on shear strength of the

7   PHC pile with large diameter. In: Proceedings of 12th World Conference on Earthquake

8   Engineering, Auckland, New Zealand.

9   Li H (2004) High strength concrete and its composite structure. Science Press, Beijing.

10   Lignola GP, Prota A, Manfredi G and Cosenza E (2017) Experimental performance of RC hollow

11   columns confined with CFRP. *ASCE Journal of Composites for Construction* **11(1)**: 42-49.

12   Muguruma H, Watanabe F and Nishiyama M (1987) Improving the flexural ductility of pretensioned

13   high strength spun concrete piles by lateral confining of concrete. In: Proceedings of the Pacific

14   Conference on Earthquake Engineering, Wairakei, New Zealand, 1: 385-396.

15   Murugan M, Muthukkumaran K and Natarajan C (2017) FRP-strengthened RC piles. I: Piles under

16   static lateral loads. *ASCE Journal of Performance of Constructed Facilities* **31(3)**: 04017003.

17   Nagae T and Hayashi S (2003) Earthquake-resistant property of prefabricated high-strength concrete

18   pile. In: Proceedings of the International Conference on High Performance Materials in Bridges,

19   Kona, Hawaii, 173-182.

20   Özden G and Akdag CT (2009) Lateral load response of steel fiber reinforced concrete model piles

21   in cohesionless soil. *Construction and Building Materials* **23(2)**: 785-794.

22   Park H, Jeong S, Lee SC and Cho JY (2016) Flexural behavior of post-tensioned prestressed concrete

29

girders with high-strength strands. *Engineering Structures* **112**: 90-99.

Paul A, Gleich LB and Kahn LF (2017) Structural performance of prestressed concrete bridge piles using duplex stainless steel strands. *ASCE Journal of Structural Engineering* **143(7)**: 04017042.

PCI (2017) PCI design handbook: precast and prestressed concrete (8th ed.). Precast/Prestressed Concrete Institute, Chicago, Illinois.

Qiao PZ, Liu QH, Lu Z and Wang ZJ (2018) Flexural behaviour of GFRP-encased concrete panels. *Magazine of Concrete Research* **70(24)**: 1265-1279.

Velasco RV (2008) Self-consolidating concretes reinforced with high volumetrics fractions of steel fibers: Rheological, Physics, Mechanics and Thermal Properties. PhD Thesis, Federal University of Rio de Janeiro, Rio de Janeiro, Brazil.

Wang WD, Li Q, Hu Y, Shi JW and Ng CWW (2017) Field investigation of collapse of a 13-story high-rise residential building in Shanghai. *ASCE Journal of Performance of Constructed Facilities* **31(4)**: 04017012.

Wee TH, Chin MS and Mansur MA (1996) Stress-strain relationship of high-strength concrete in compression. *ASCE Journal of Materials in Civil Engineering* **8(2)**: 70-76.

Wu P, Guo Y, Zhu DY, Jin WL, Zhang ZH and Liang RZ (2020) Flexural performances of prestressed high strength concrete piles reinforced with hybrid GFRP and steel bars. *Marine Georesources and Geotechnology* **38(5)**: 518-526.

Yang ZJ, Li GC and Wang WJ (2018b) Experimental investigation and nonlinear finite element analysis on seismic performance of PHC piles. *Structural Engineering International* **28(4)**: 475-488.

Yang ZJ, Li GC, Wang WJ and Lv YJ (2018a) Study on the flexural performance of prestressed high

30

strength concrete pile. *KSCE Journal of Civil Engineering* **22(10)**: 4073-4082.

Yilmaz T, Arslan B and Anil Ö (2019) Nonlinear FEA of mechanical anchorages on CFRP-to-concrete

bonded joint. *Magazine of Concrete Research* **71(9)**: 488-502.

Yu XD and Gao JH (2016) Fixed device, manufacturing equipment and manufacturing methods for

manufacturing steel strand and reinforcing bar cages. CN105464107A.

Zhang XZ, Niu SX, Yan JB and Zhang SH (2019) Seismic behaviour of prestressed high-strength

concrete piles under combined axial compression and cyclic horizontal loads. *Advances in*

Structural Engineering **22(5)**: 1089-1105.

31
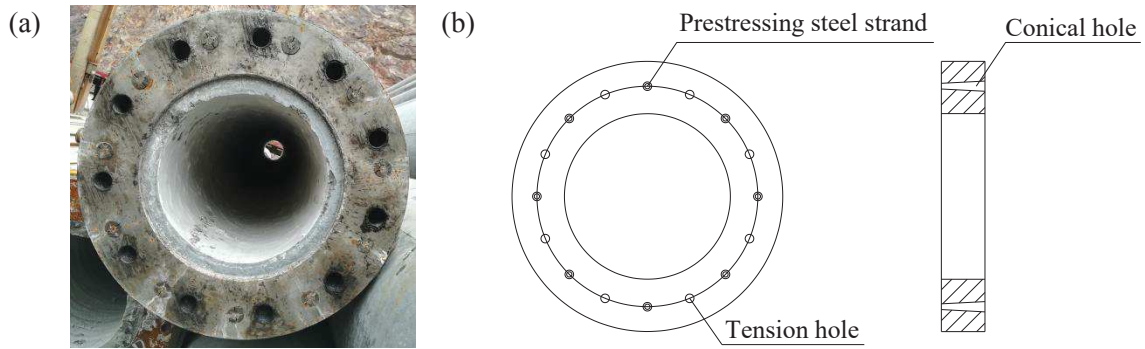
Figure 1. End plate for anchorage of pretensioned steel strands: (a) photo of end plate; (b)

schematic diagram
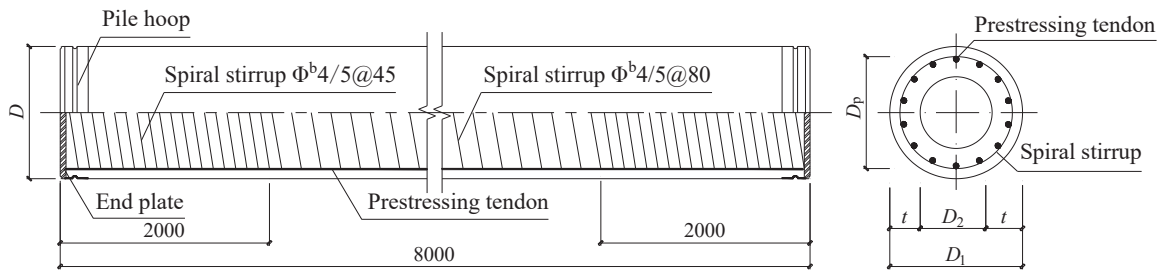
Figure 2. Schematic diagram of reinforcements in test specimens (Unit: mm)

32
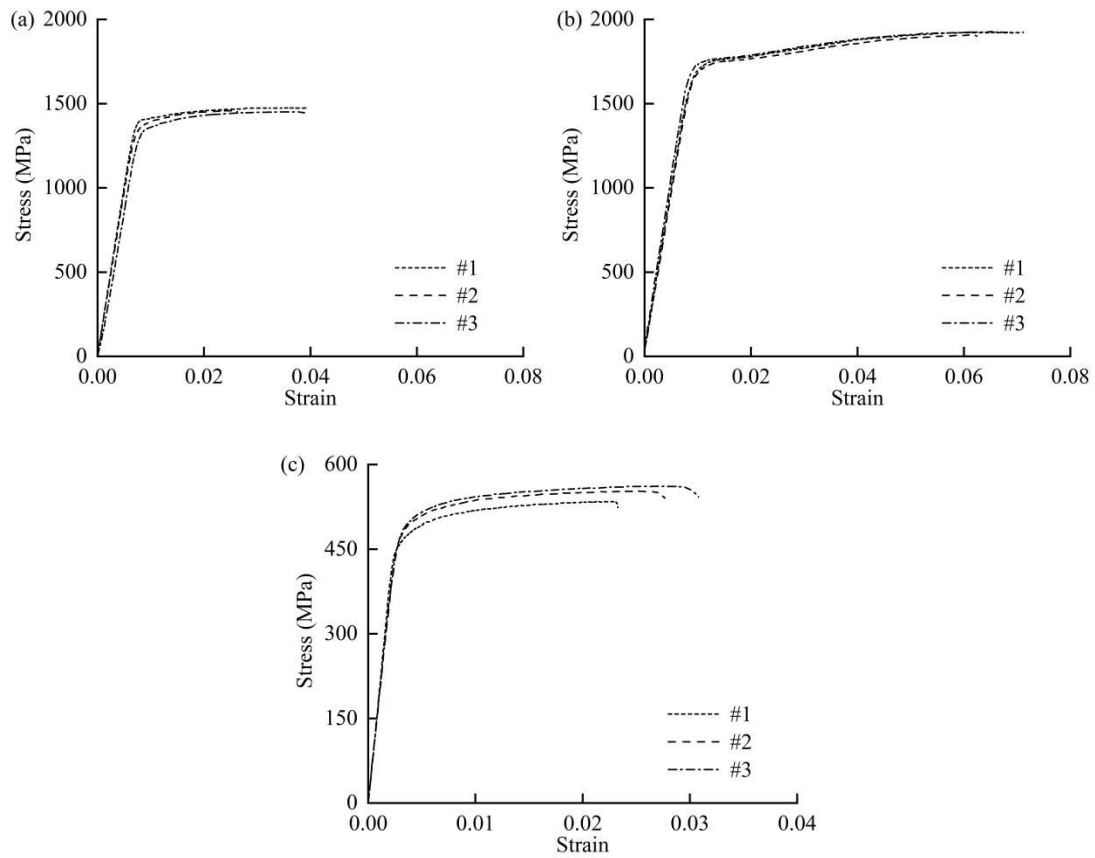
Figure 3. Measured stress-strain curves of reinforcing bars: (a) $\Phi^D 10.7$; (b) $\Phi^S 11.1$; (c) $\Phi^b 6$

33

(a)

(b)
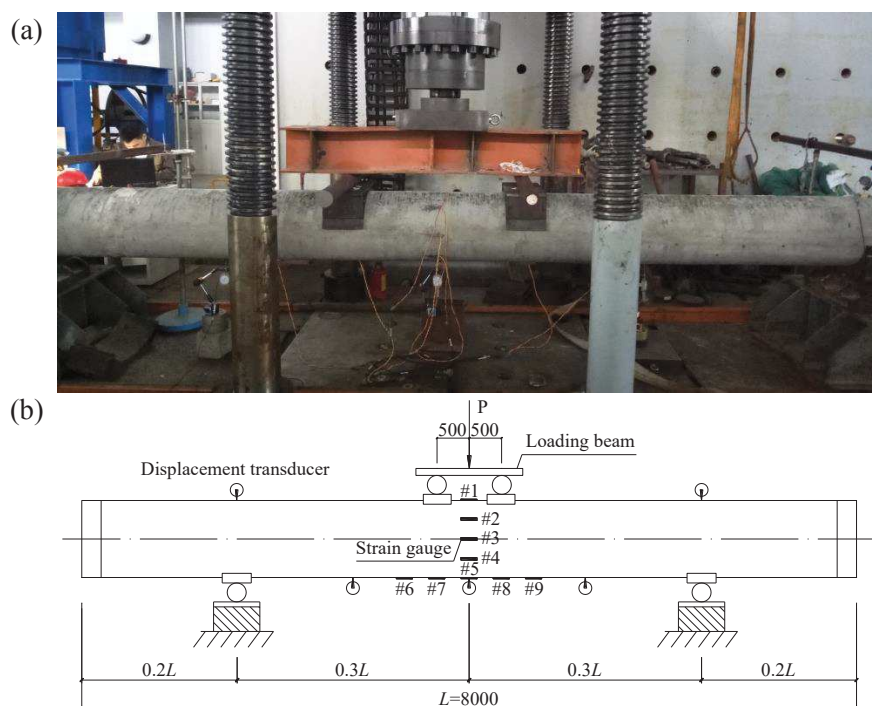
Figure 4. Bending test setup and loading scheme: (a) setup photo; (b) schematic diagram (Unit: mm)

34
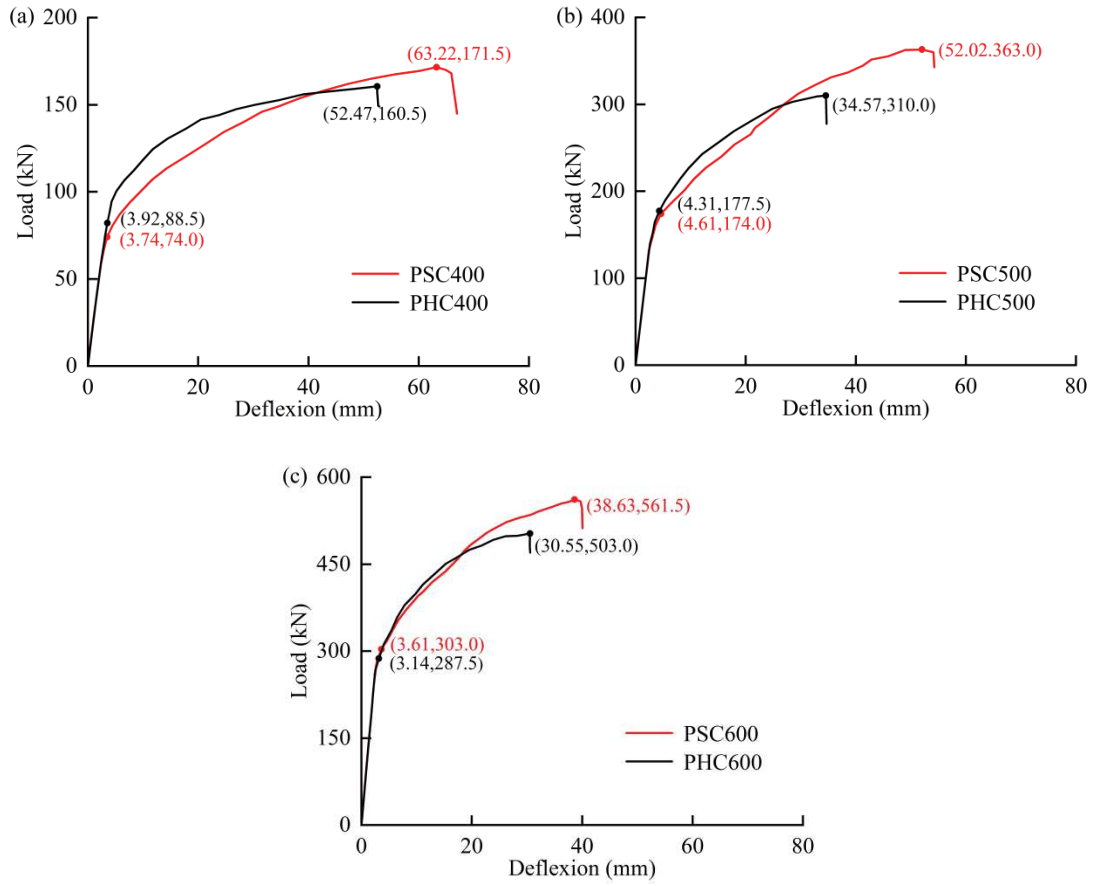
Figure 5. Load vs. midspan deflexion curves of test specimens
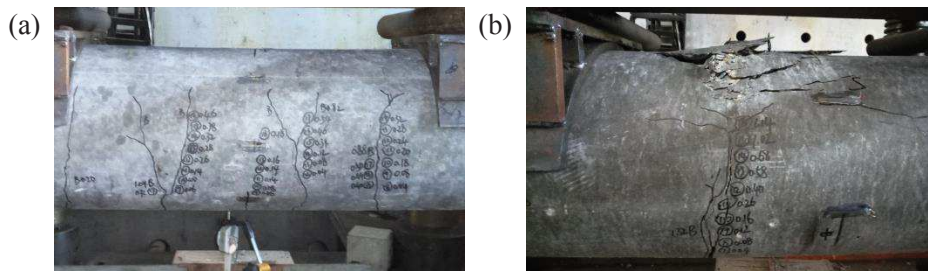
Figure 6. Failure modes of test specimens: (a) PHC400; (b) PSC400

35
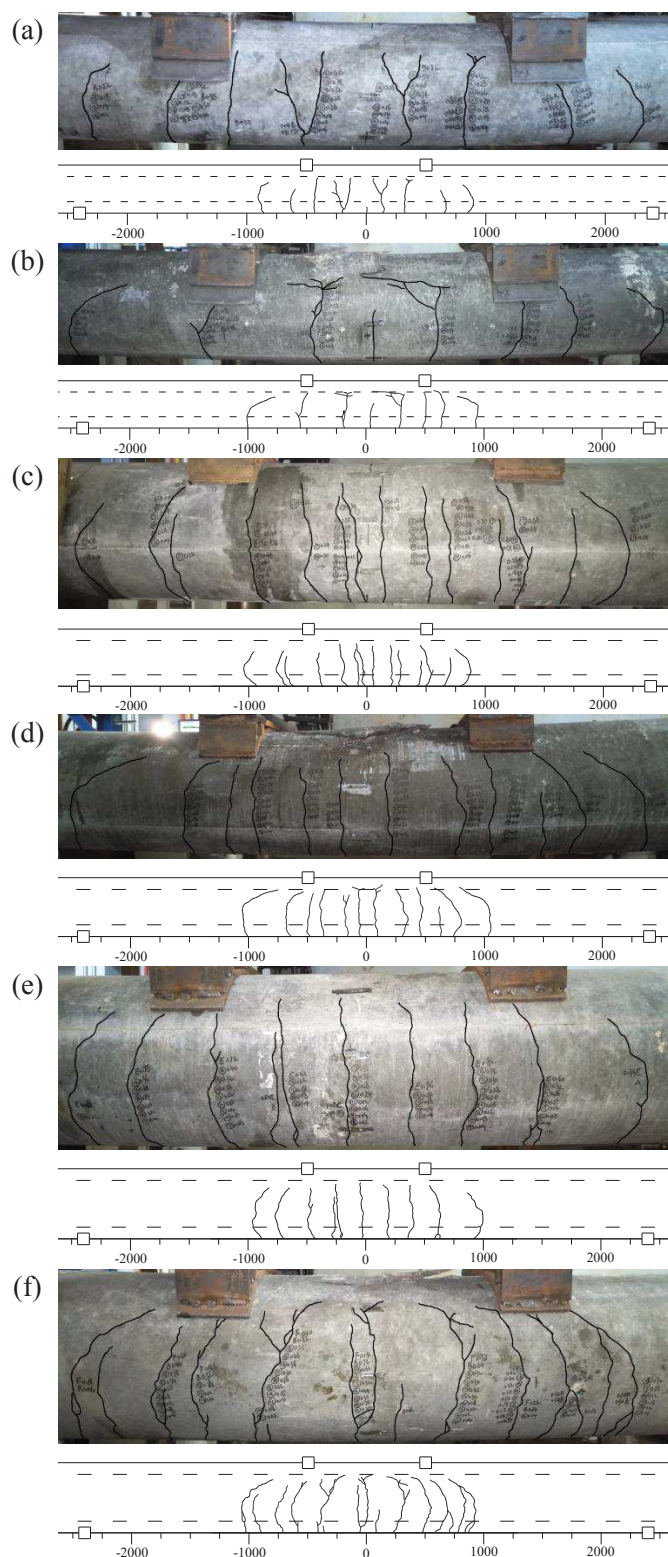
Figure 7. Crack distribution of test specimens: (a) PHC400; (b) PSC400; (c) PHC500; (d) PSC500;

(e) PHC600; (f) PSC600

36
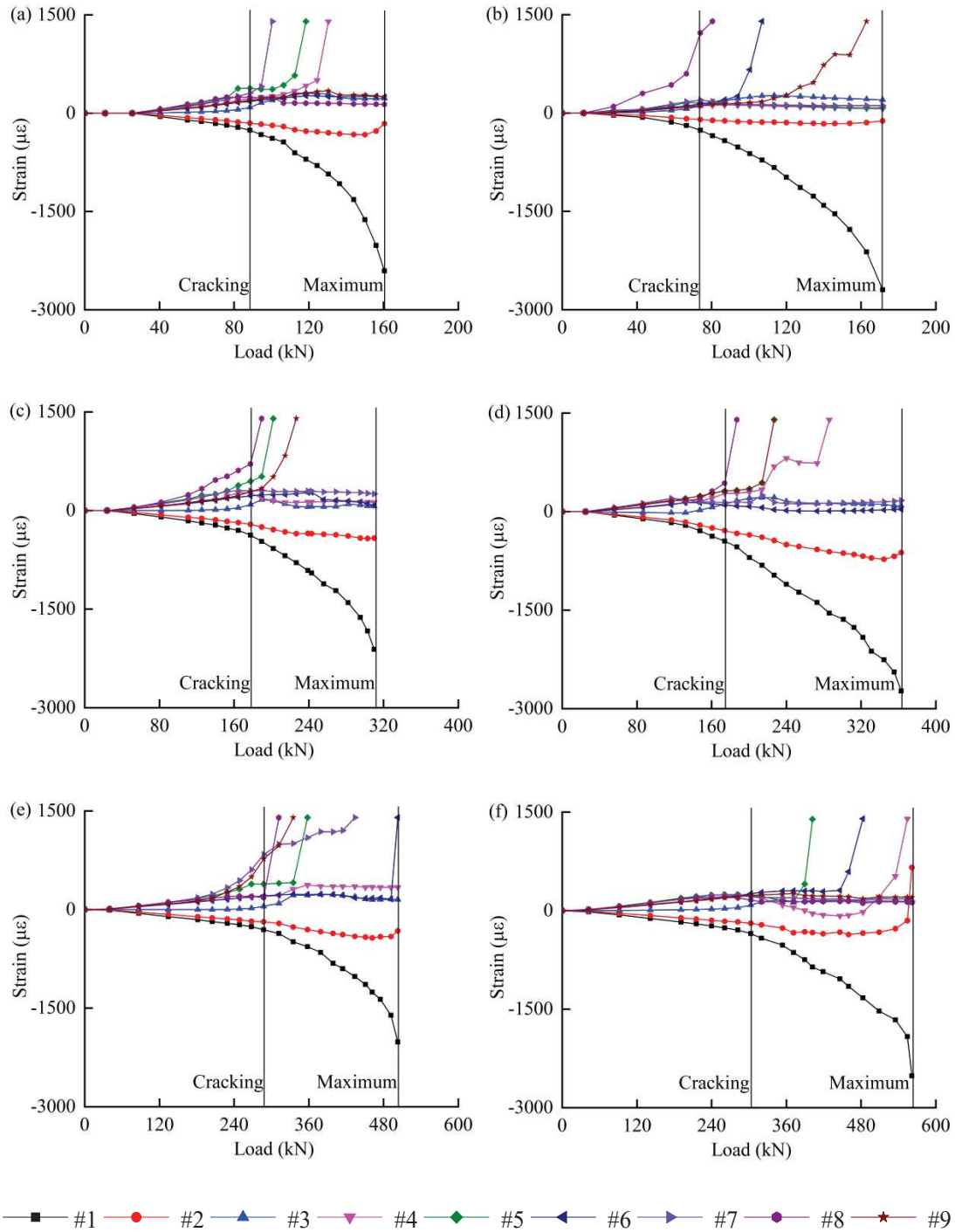
Figure 8. Concrete strain development of test specimens: (a) PHC400; (b) PSC400; (c) PHC500;

(d) PSC500; (e) PHC600; (f) PSC600

37
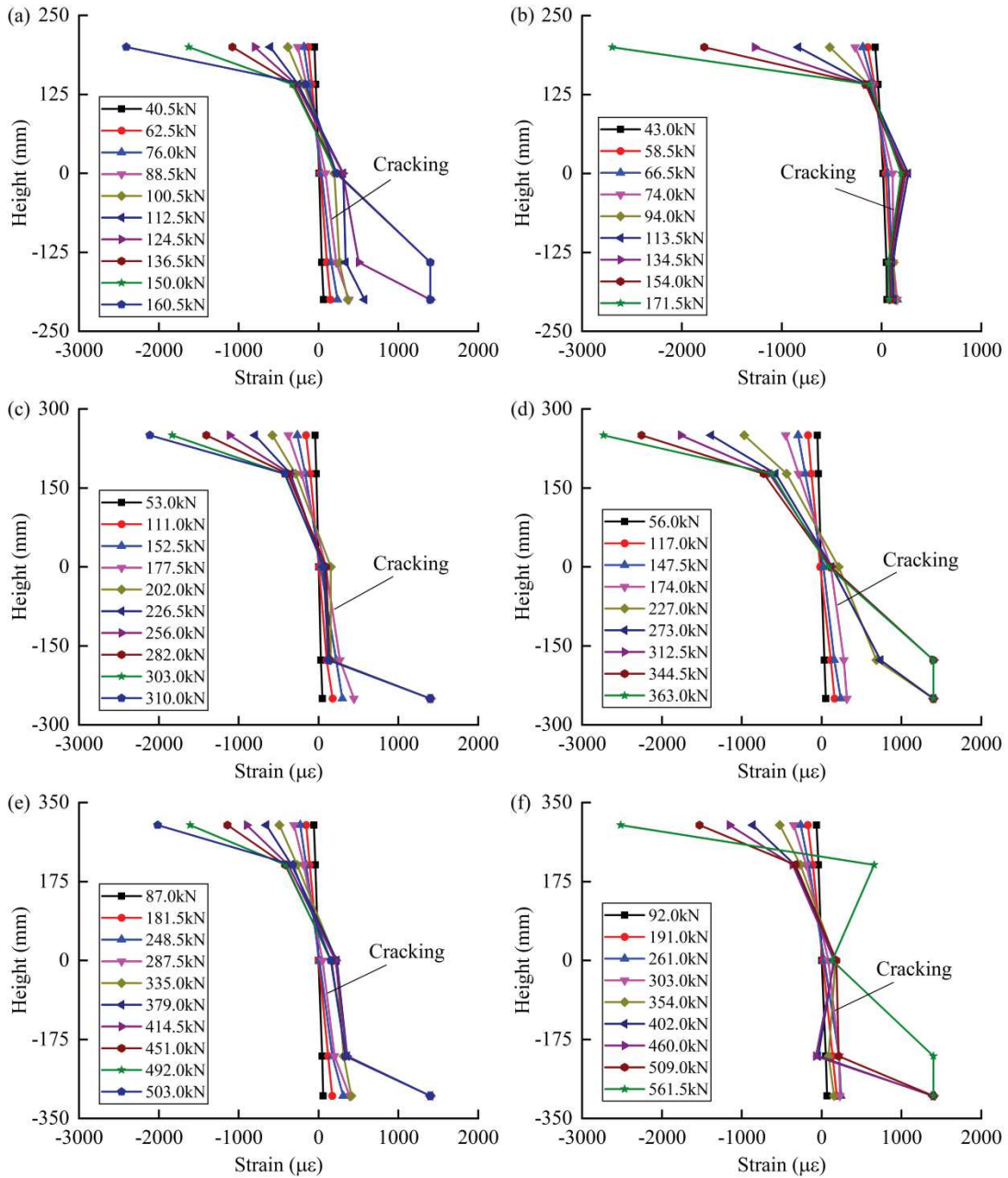
Figure 9. Concrete strain distribution over the depth of the midspan section: (a) PHC400; (b) PSC400; (c) PHC500; (d) PSC500; (e) PHC600; (f) PSC600

38
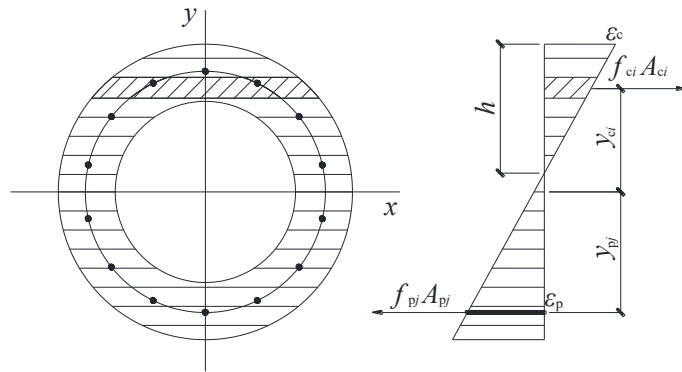
**Figure 10.** Pile cross-section and strain distribution for the general bending analysis
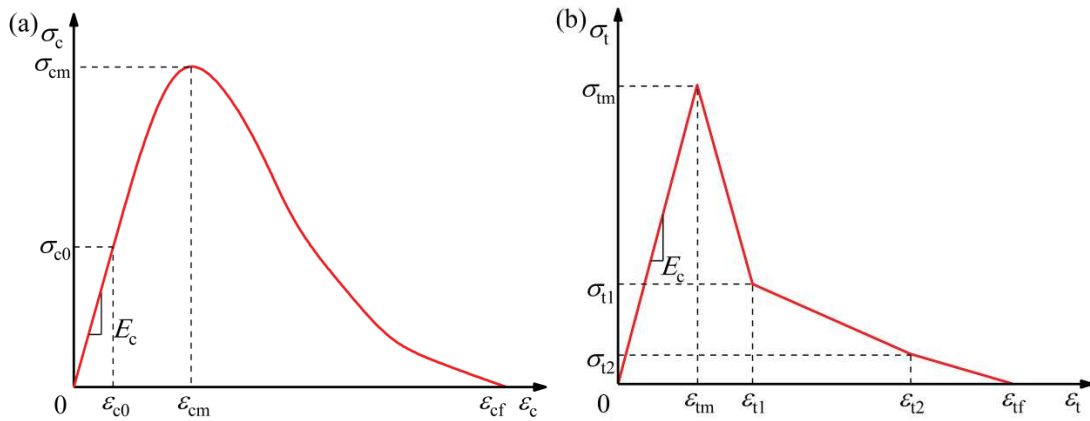
Figure 11. Stress-strain curves of concrete: (a) uniaxial compression; (b) uniaxial tension

39
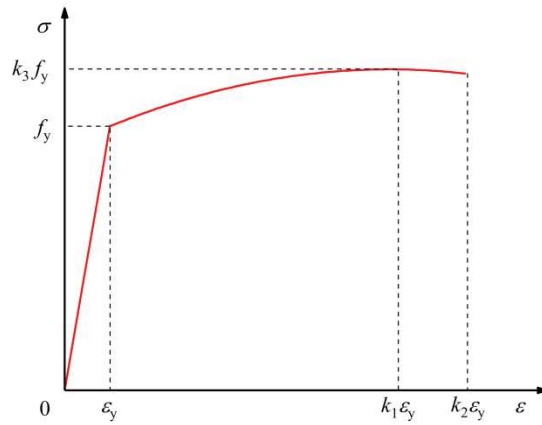
Figure 12. Stress-strain curve of reinforcing bar under uniaxial tension
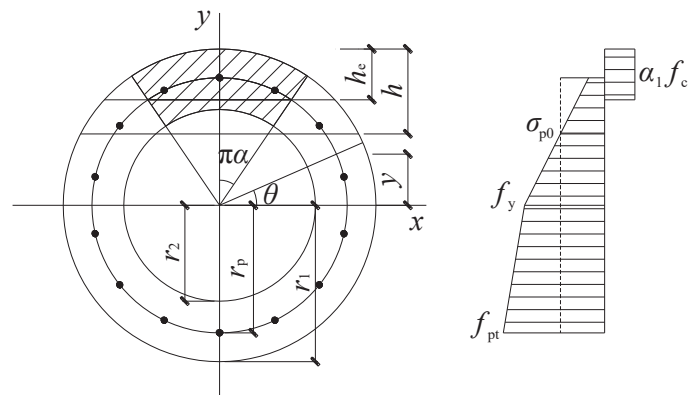
Figure 13. Cross-section stress distribution for the simplified calculation method

40
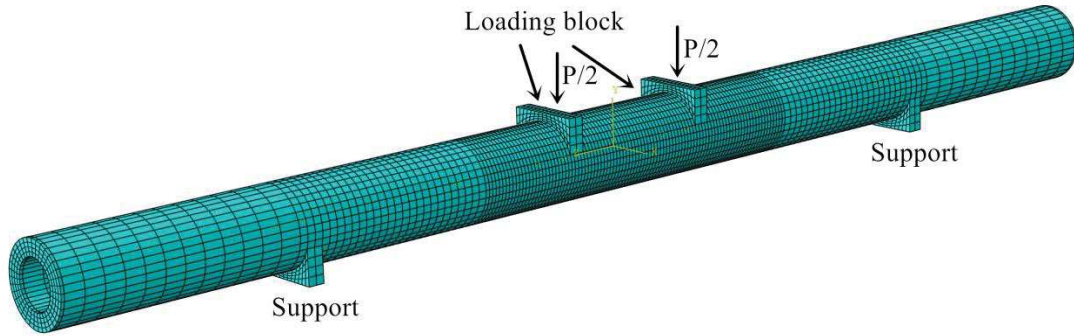
Figure 14. Schematic diagram of finite element model
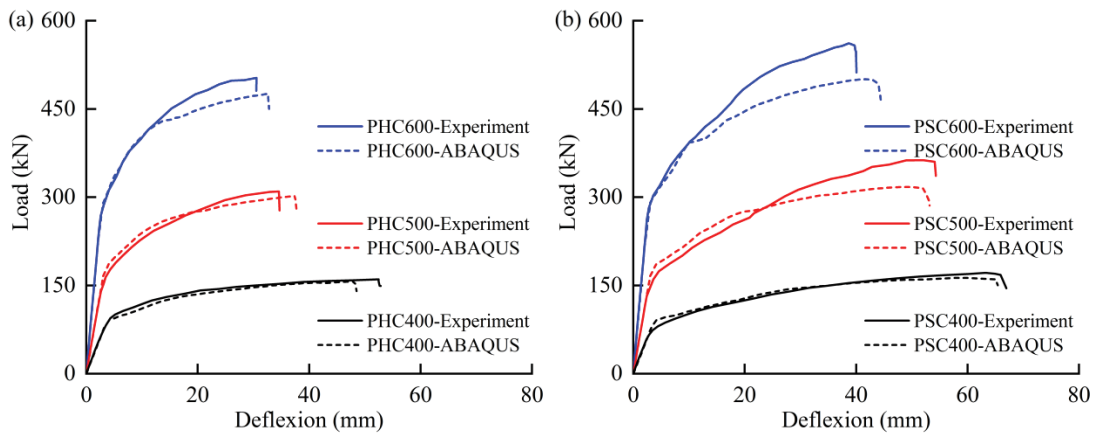
Figure 15. Comparison of load-deflexion curves between numerical and experimental results

41
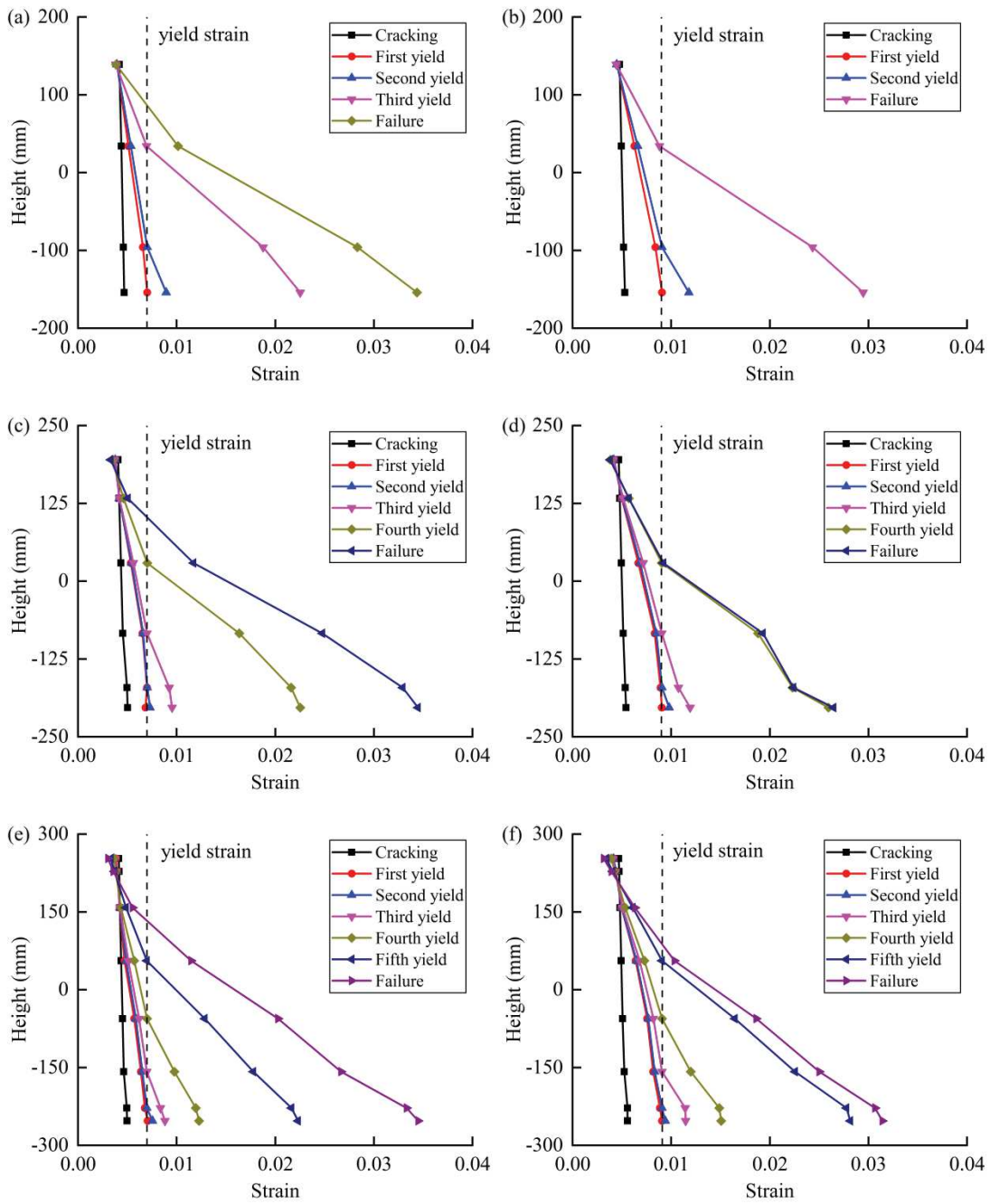
Figure 16. Strain distribution of prestressing tendons over the cross-section depth in the midspan section: (a) PHC400; (b) PSC400; (c) PHC500; (d) PSC500; (e) PHC600; (f) PSC600

42
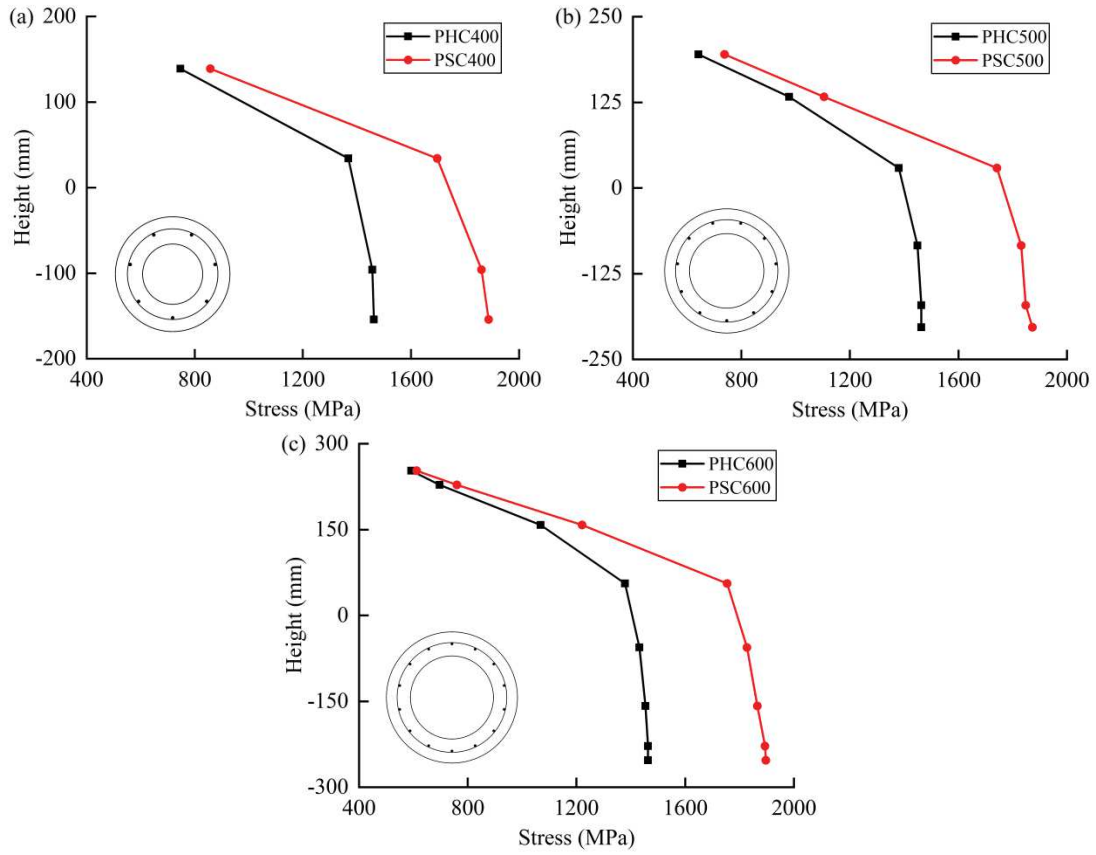
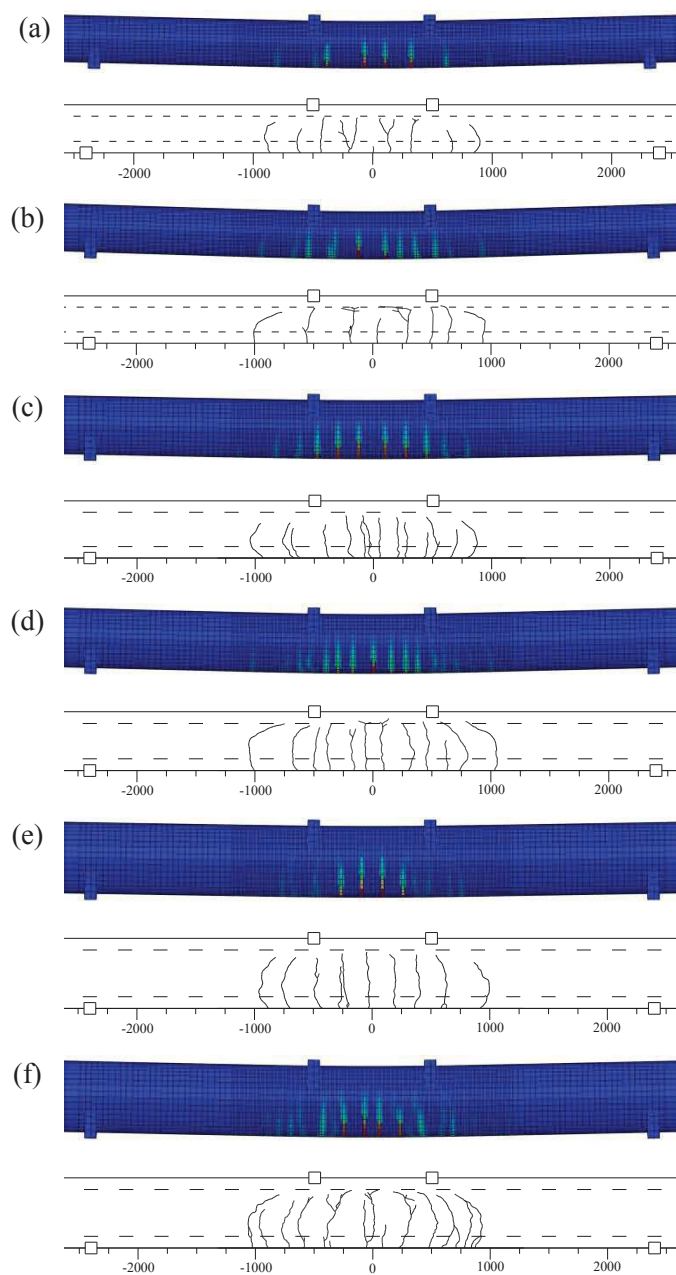**Figure 17.** Stress distribution of prestressing tendons along the height of the midspan cross-section

at failure

43

Figure 18. Crack distribution of numerical and experimental results for test specimens: (a) PHC400; (b) PSC400; (c) PHC500; (d) PSC500; (e) PHC600; (f) PSC600

44

Table 1. Geometric dimensions and reinforcement specifications of test specimens

Pile type	D_1 (mm)	D_p (mm)	t (mm)	Longitudinal reinforcement	ρ_s (%)	Stirrup	σ_{con} (MPa)	σ_{ce} (MPa)
PHC400	400	308	95	$7\Phi^D10.7$	0.69	$\Phi^b4@45/80$	994	5.99
PSC400	400	308	95	$7\Phi^S11.1$	0.57	$\Phi^b4@45/80$	1302	5.57
PHC500	500	406	100	$11\Phi^D10.7$	0.79	$\Phi^b5@45/80$	994	6.74
PSC500	500	406	100	$11\Phi^S11.1$	0.65	$\Phi^b5@45/80$	1302	6.31
PHC600	600	506	110	$14\Phi^D10.7$	0.74	$\Phi^b5@45/80$	994	6.40
PSC600	600	506	110	$14\Phi^S11.1$	0.61	$\Phi^b5@45/80$	1302	5.98

Table 2. Material mechanical parameters of reinforcing bars

Reinforcing bar	E_s (GPa)	f_y (MPa)	f_u (MPa)	δ (%)
$\Phi^D10.7$	195	1342	1462	3.4
$\Phi^S11.1$	195	1725	1920	6.4
Φ^b6	199	477	549	2.6

Table 3. Comparison of flexural performance of test specimens

Pile type	$M_{cr,e}$ (kN·m)	$M_{cr,e,PSC}/M_{cr,e,PHC}$	$M_{u,e}$ (kN·m)	$M_{u,e,PSC}/M_{u,e,PHC}$	$f_{u,e}$ (mm)	$f_{u,e,PSC}/f_{u,e,PHC}$
PHC400	87.6		156.0		52.47	
PSC400	73.8	0.84	166.5	1.07	63.22	1.20
PHC500	173.5		299.4		34.57	
PSC500	170.1	0.98	349.8	1.17	52.02	1.50
PHC600	279.8		484.9		30.55	
PSC600	294.5	1.05	540.0	1.11	38.63	1.26

Table 4. Comparison between theoretical and experimental results

Pile type	Experiment	General calculation method			Simplified calculation method		
	$M_{u,e}$ (kN·m)	h_g (mm)	$M_{u,g}$ (kN·m)	$M_{u,g}/M_{u,e}$	h_s (mm)	$M_{u,s}$ (kN·m)	$M_{u,s}/M_{u,e}$
PHC400	156.0	80.0	140.7	0.90	84.7	130.3	0.84
PSC400	166.5	74.0	147.5	0.89	85.6	139.0	0.83
PHC500	299.4	97.5	275.3	0.92	95.9	268.5	0.90
PSC500	349.8	91.0	291.1	0.83	97.7	286.5	0.82
PHC600	484.9	108.6	432.3	0.89	99.1	427.5	0.88
PSC600	540.0	101.4	457.0	0.85	101.1	456.1	0.84

45

Table 5. Material parameter values of reinforcing bars

Reinforcing bar	E_s (GPa)	f_y (MPa)	ε_y	k_1	k_2	k_3
$\Phi^D 10.7$	195	1342	0.0069	4.93	5.22	1.09
$\Phi^S 11.1$	195	1725	0.0088	7.16	7.83	1.11
$\Phi^b 4/5$	199	477	0.0024	10.8	12.1	1.15

Table 6. Comparison of flexural performance between numerical and experimental results

Pile type	$M_{cr,n}$ (kN·m)	$M_{cr,e}$ (kN·m)	$M_{cr,n}/M_{cr,e}$	$M_{u,n}$ (kN·m)	$M_{u,e}$ (kN·m)	$M_{u,n}/M_{u,e}$	$f_{u,n}$ (mm)	$f_{u,e}$ (mm)	$f_{u,n}/f_{u,e}$
PHC400	89.8	87.6	1.03	152.4	156.0	0.98	48.21	52.47	0.92
PSC400	89.6	73.8	1.21	158.4	166.5	0.95	59.71	63.22	0.94
PHC500	172.8	173.5	1.00	291.8	299.4	0.97	37.49	34.57	1.08
PSC500	174.6	170.1	1.03	306.6	349.8	0.88	48.95	52.02	0.94
PHC600	270.3	279.8	0.97	458.7	484.9	0.95	32.63	30.55	1.07
PSC600	274.3	294.5	0.93	482.3	540.0	0.89	41.20	38.63	1.07

46